Chiral microresonator assisted by Rydberg-atom ensembles

Xiao-Fei Liu,[1] Tie-Jun Wang,[1] Yong-Pan Gao,[1] Cong Cao,[2] and Chuan Wang[1,3,*]

[1]*State Key Laboratory of Information Photonics and Optical Communications and School of Science,*
Beijing University of Posts and Telecommunications, Beijing 100876, China
[2]*School of Ethnic Minority Education, Beijing University of Posts and Telecommunications, Beijing 100876, China*
[3]*College of Information Science and Technology, Beijing Normal University, Beijing 100875, China*

The chiral light-matter interaction, which shows great potential in applications ranging from photonic devices to quantum information processing, can be achieved with the development of recent experimental advances of the fabrication technologies on nanoscales. Traditionally, the chiral optics based on spin-momentum locking in micro- and nanophotonics could be observed only for specific optical modes, such as the transverse magnetic mode. Here in this study, we investigate that the chirality of a whispering-gallery-mode (WGM) microresonator can be well controlled with assistance from coupled Rydberg-atom ensembles. The presented asymmetric backscattering also originates from interferences between scattered optical modes in the WGM microresonator, which is proposed by Wiersig [Phys. Rev. A **84**, 063828 (2011)]. Therefore the flow of light can be well controlled, and the statistical properties of photons could be changed by regulating this asymmetric coupling. Most importantly, its universal chiral property is not limited by specific optical modes which may also be used as optical diodes and routers.

I. INTRODUCTION

Chirality which describes the mirror-symmetric property of a system plays an important role in modern physics. It can be observed in many phenomena and systems which involve the symmetry, such as the quantum Hall effect [1], Higgs boson physics [2], double-well Bose-Einstein condensates [3], topological insulators [4], and superconductors [5]. As the property of photons is similar with electrons, the concept of chirality can also be extended to optical domains. Recently, as a result of experimental advances in fabricating micro- and nanophotonic structures, chiral quantum optics has become possible and been achieved in experiments [6]. For example, the time-reversal symmetry of Maxwell's equations gives rise to a transverse spin component of photons and the spin-momentum locking in strongly confined optical fields [7–9]. This transverse spin will flip its sign if the propagation direction of the optical field is reversed. Meanwhile, when this spin-momentum locking optical field interacts with a dipole emitter supporting both the σ_+ and σ_- transition, the nonreciprocal transmission can be achieved due to this chiral light-matter interaction [10–16].

During the past decades, there has been remarkable progress in the study of ultrahigh-quality factor Q microcavities which could greatly improve the performance of light-matter interaction [17–21]. Specifically, the whispering-gallery-mode (WGM) microresonators [22,23], in which light travels through internal total reflection, have a Q factor larger than 10^8 and small mode volumes in microscales. They have been widely used in ultralow-threshold micro- and nanolaser [24–26], parity-time (PT) symmetric or antisymmetric optics

[27–31], cavity quantum electrodynamics (C-QED) [32], optomechanics [33–37], nonlinear optics [38–40], ultralong photon storage [41], and ultrasensitive detections [42–44]. Meanwhile, the chiral light-matter interaction can be controlled at the single-photon level, with potential applications in quantum information processing. More recently, the quantum optical circulator [45], single-photon isolation [46], and all-optical quantum router [15] which are based on the chiral light-matter interaction have been achieved in WGM microcavities coupled with the cold ^{87}Rb atoms. The WGM microcavities, like microsphere or microtoroid, support both the TE and TM modes. However, only the TM mode can exhibit this chiral light-matter interaction and spin-momentum locking phenomenon. Therefore these chiral photonic devices are dependent on the polarization of input light, which may limit their further applications.

Another method to achieve the universal chiral optics is to construct a non-Hermitian system [47–53] which originates from the energy or information exchange between the system and environment. In WGM microcavities, the existence of one nanoparticle around the evanescent field could induce the coherent backscattering between two counterpropagating modes. The mode splitting becomes more complicated when multi-Rayleigh scatterers exist simultaneously [49–56]. In 2011, Wiersig [49] proposed that two or more particles could lead to the appearance of exceptional points (EPs) and asymmetric backscattering between counterpropagating optical modes. This phenomenon results from destructive or constructive interference of the scattered optical modes. Subsequently, this system is found to be used to enhance the detection sensitivity of particles [50,51]; meanwhile, asymmetric backscattering, EPs, and sensitive detections are observed in experiments [52–54].

---

*wangchuan@bupt.edu.cn

In this paper, we will show a precise control of chiral matter-light interaction and asymmetric backscattering assisted by Rydberg-atom ensembles. The asymmetric backscattering in this paper also originates from interferences between different scattered modes in non-Hermitian systems, which is proposed by Wiersig [49]. The difference is that we can control chiral properties of optical fields through changing the input frequency and strength of an external control field acting on Rydberg atoms while keeping the position (or phase) of the atom ensembles unchanged. In this model, the energy level of the Rydberg atom is the standard Λ-type configuration, which couples with both the cavity mode and the external classical control field. After adiabatically eliminating the excited state of the Rydberg atom, the Stark shift and coupling strength between the atom and cavity mode can be well controlled. Furthermore, the asymmetric backscattering which is quantized by the chirality parameter D could be achieved. Meanwhile, statistical properties of photons are also determined by this chiral property, and an analytical expression of the equal-time second-order correlation function $g^{(2)}(0)$ is derived when the pump driving is weak.

This paper is organized as follows. In Sec. II, we show the model and the adiabatic elimination of excited states of Rydberg atoms. Furthermore, the Hamiltonian is transformed into the interaction between four boson fields using the Holstein-Primakoff transformation. In Sec. III, the model is further simplified into the interaction between two counterpropagating optical modes by eliminating atom ensembles. The chirality of this system is also analyzed in detail. Section IV discusses statistical properties of photons. Finally, we give the summary and further discussions.

II. THEORETICAL MODEL

Consider the system that contains a WGM microtoroid coupled with Rydberg-atom ensembles and add-drop–type taper fiber, as shown in Fig. 1(a). The WGM microtoroid supports both the clockwise (CW) and counterclockwise (CCW) optical mode, which are described by the bosonic annihilation operator $\hat{a}_{cw}$ ($\hat{a}_{ccw}$) and creation operator $\hat{a}_{cw}^\dagger$ ($\hat{a}_{ccw}^\dagger$). These two modes (both TE or TM mode) have the same resonant frequency ω_c and dissipation rate κ. Figure 1(b) shows the Λ-type energy levels of the atom, which are represented by $|e_k^j\rangle$, $|g_k^j\rangle$, and $|f_k^j\rangle$ for the kth atom in the jth ensemble. The $|e_k^j\rangle \leftrightarrow |g_k^j\rangle$ transition is driven by an external control field with central frequency ω_p^j, while the transition $|e_k^j\rangle \leftrightarrow |f_k^j\rangle$ interacts with degenerate CW and CCW modes with coupling strength J_j. The total number of Rydberg atoms in the jth ensemble is N_j.

The Hamiltonian of this system could be described as $\hat{H} = \hat{H}_c + \hat{H}_a + \hat{H}_I$, where $\hat{H}_c$ is the Hamiltonian of the optical WGM field which has the expression $\hat{H}_c = \omega_c(\hat{a}_{cw}^\dagger \hat{a}_{cw} + \hat{a}_{ccw}^\dagger \hat{a}_{ccw})$ by setting $\hbar = 1$. The second term $\hat{H}_a = \sum_{j,k}(\omega_g \sigma_{gg}^{jk} + \omega_e \sigma_{ee}^{jk} + \omega_f \sigma_{ff}^{jk})$ describes the Hamiltonian of atoms in which $\sigma_{gg}^{jk} = |g_k^j\rangle\langle g_k^j|$, $\sigma_{ee}^{jk} = |e_k^j\rangle\langle e_k^j|$, and $\sigma_{ff}^{jk} = |f_k^j\rangle\langle f_k^j|$ stand for the corresponding transitions of the kth atom in the jth ensemble. The interaction Hamiltonian $\hat{H}_I$ represents the coupling between atoms and optical fields
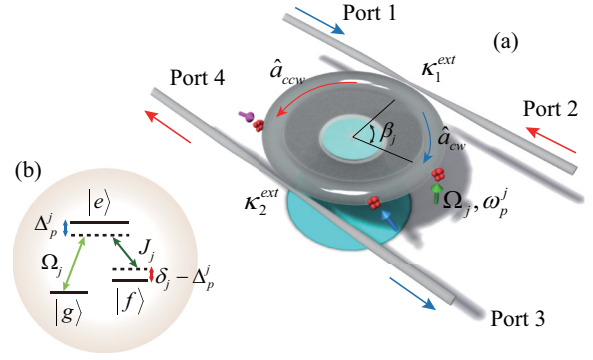
FIG. 1. (a) Illustration of microtoroid coupled with Rydberg-atom ensembles. Meanwhile, this microtoroid also couples with two taper fibers, forming the add-drop structure. The phase of the jth ensemble is represented by β_j. When a probe signal is input from port 1 (or port 2), the transmission is detected from port 3 (or port 4), i.e., port 1 → port 3 (or port 2 → port 4). The intrinsic dissipation rate of the microtoroid is κ_0, and the coupling strengths with these two taper fibers are κ_1^{ext} and κ_2^{ext}, respectively. (b) The energy level of the Rydberg atom and its interaction with the cavity modes $\hat{a}_{cw(ccw)}$ and the external control laser.

which is expressed as

$$\hat{H}_I = \sum_{j,k} \left[J_i \sigma_{ef}^{jk}(\hat{a}_{cw}e^{i\beta_j} + \hat{a}_{ccw}e^{-i\beta_j}) + \Omega_j \sigma_{eg}^{jk}e^{-i\omega_p^j t} + \text{H.c.} \right].$$

(1)

Here, $\sigma_{ef}^{jk} = |e_k^j\rangle\langle f_k^j|$ and $\sigma_{eg}^{jk} = |e_k^j\rangle\langle g_k^j|$, which correspond to the transition from the $|f_k^j\rangle$ state (or $|g_k^j\rangle$ state) to the $|e_k^j\rangle$ state. For simplification, we assume that the size of each atom ensemble is small enough so that different atoms within one ensemble have the same coupling strength J_j and Ω_j together with the same phase β_j. By applying the unitary evolution operation $\hat{U}(t) = \mathcal{T}\exp\{-i(\hat{H}_a + \hat{H}_c)t\}$, the total Hamiltonian can be transformed into an interaction picture using the formula $\hat{H}_I^{(1)} = \hat{U}^\dagger(t)\hat{H}\hat{U}(t) - i\hat{U}^\dagger(t)\partial\hat{U}(t)/\partial t$, which becomes

$$\hat{H}_I^{(1)} = \sum_{j,k} \left[J_j \sigma_{ef}^{jk}(\hat{a}_{cw}e^{i\beta_j} + \hat{a}_{ccw}e^{-i\beta_j})e^{i\delta_j t} \right.$$
$$\left. + \Omega_j \sigma_{eg}^{jk}e^{i\Delta_p^j t} + \text{H.c.} \right].$$

(2)

Here, the effective detunings are $\Delta_p^j = \omega_e - \omega_g - \omega_p^j$ and $\delta_j = \omega_e - \omega_f - \omega_c$. When they are much larger than the corresponding coupling strength, i.e., $\delta_j, \Delta_p^j \gg J_j, \Omega_j$, the excited states can be adiabatically eliminated. Then we transform the Hamiltonian into the noninteracting picture again, and it becomes $\hat{H}^{(2)} = \hat{H}_a^{(2)} + \hat{H}_c^{(2)} + \hat{H}_I^{(2)}$. Apparently, $\hat{H}_c^{(2)}$ stays unchanged while $\hat{H}_a^{(2)}$ and $\hat{H}_I^{(2)}$ have the expression as

$$\hat{H}_a^{(2)} = \sum_{j,k} \left[\left(\omega_g - \frac{\Omega_j^2}{\Delta_p^j} \right)\sigma_{gg}^{jk} + \left(\omega_f - \frac{J_j^2}{\Delta_p^j}\hat{n} \right)\sigma_{ff}^{jk} \right]$$

(3)

and

$$\hat{H}_I^{(2)} = \sum_{j,k} \left[-\frac{\Omega_j J_j}{\Delta_p^j}\sigma_{gf}^{jk}(\hat{a}_{cw}e^{i\beta_j} + \hat{a}_{ccw}e^{-i\beta_j})e^{-i\omega_p^j t} + \text{H.c.} \right],$$

(4)

with $\hat{n} = \hat{a}_{cw}^{\dagger}\hat{a}_{cw} + \hat{a}_{ccw}^{\dagger}\hat{a}_{ccw}$. The average value $\langle\hat{n}\rangle$ represents the number of photons inside this microresonator. From Eq. (3), it is clearly seen that the energy level of the $|g_k^j\rangle$ and $|f_k^j\rangle$ state have changes of $-\Omega_j^2/\Delta_p^j$ and $-J_j^2\hat{n}/\Delta_p^j$, respectively.

Then we introduce the collective spin operator given by $S_j^+ = \sum_{k=1}^{N_j}\sigma_{fg}^{jk}$ and $S_j^- = \sum_{k=1}^{N_j}\sigma_{gf}^{jk}$. The S_j^+ and S_j^- operators could be transferred into the bosonic mode $\hat{b}_j$ using the Holstein-Primakoff (HP) transformation, i.e., $S_i^+ = \hat{b}_j^{\dagger}(N_j - \hat{b}_j^{\dagger}\hat{b}_j)^{1/2}$ and $S_j^- = (N_j - \hat{b}_j^{\dagger}\hat{b}_j)^{1/2}\hat{b}_j$. When the mean number of excitations is much less than the total number of atoms, i.e., $\langle\hat{b}_j^{\dagger}\hat{b}_j\rangle \ll N_j$, the collective spin operator can be further simplified into $S_j^+ \simeq \sqrt{N_j}\hat{b}_j^{\dagger}$ and $S_j^- \simeq \sqrt{N_j}\hat{b}_j$.

For convenience, $\hat{H}^{(2)}$ is rewritten as $\hat{H}$ in the following. As shown in Fig. 1(a), the CW mode of the microtoroid is pumped by the field with strength ε and frequency ω_c^{in}. In the rotating reference frame, the total Hamiltonian becomes $\hat{H} = \hat{H}_0 + \hat{H}_I + \hat{H}_{\text{drive}}$. If this system is excited from port 1, the driving term has the expression $\hat{H}_{\text{drive}} = \sqrt{\kappa_1^{\text{ext}}}(\varepsilon\hat{a}_{cw} + \varepsilon^*\hat{a}_{cw}^{\dagger})$. Here, $\hat{H}_0 = \Delta_c(\hat{a}_{cw}^{\dagger}\hat{a}_{cw} + \hat{a}_{ccw}^{\dagger}\hat{a}_{ccw}) + \sum_j \Delta_j\hat{b}_j^{\dagger}\hat{b}_j$, which represents the Hamiltonian of two counterpropagating optical fields and Rydberg-atom ensembles. The detuning Δ_c is $\omega_c - \omega_c^{\text{in}}$ and Δ_j has the expression $\omega_f - \omega_g + \Omega_j^2/\Delta_p^j - \omega_p^j - \omega_c^{\text{in}}$ under the condition $J_j^2\langle\hat{n}\rangle/\Delta_p^j \ll \omega_f$. The interaction term $\hat{H}_I$ could be written as

$$\hat{H}_I = \sum_j G_j(\hat{a}_{cw}\hat{b}_j^{\dagger}e^{i\beta_j} + \hat{a}_{ccw}\hat{b}_j^{\dagger}e^{-i\beta_j}) + \text{H.c.}, \qquad (5)$$

where this coupling strength G_j has the expression as $-\sqrt{N_j}\Omega_j J_j/\Delta_p^j$. Generally, the coupling strength J_j and the phase β_j can only be controlled by changing the position of atom ensembles. However, since the atom ensemble is in nanoscales, this position is hard to change precisely. Fortunately, Eq. (5) demonstrates that when the excited state is adiabatically eliminated, the effective coupling strength G_j between optical modes and Rydberg atoms is not only determined by the original strength J_j, but also depends on Rabi frequency Ω_j, the detuning Δ_p^j, and the number of atoms N_j. This suggests that we can continuously tune the atom-cavity coupling by changing the external laser acting on atom ensembles while keeping the position of atom ensembles unchanged, which is much more easily operated in experiment.

III. CHIRAL LIGHT-MATTER INTERACTION ENGINEERED ASYMMETRIC BACKSCATTERING

From the above analysis, a simplified model describing the interaction between counterpropagating optical fields and Rydberg-atom ensembles is obtained. Here the coupling strength G_j between optical fields and Rydberg atoms can be effectively controlled through changing the input frequency and strength of external control field after the excited state of the Rydberg atom is adiabatically eliminated. When we neglect the driving term of this system, the dynamics of bosonic operators have the following expression in the Heisenberg

picture after taking the dissipation into consideration and neglecting quantum noise terms:

$$\frac{d\hat{a}_{cw}}{dt} = \left(-i\Delta_c - \frac{\kappa}{2}\right)\hat{a}_{cw} - i\sum_j G_j\hat{b}_je^{-i\beta_j}, \qquad (6)$$

$$\frac{d\hat{a}_{ccw}}{dt} = \left(-i\Delta_c - \frac{\kappa}{2}\right)\hat{a}_{ccw} - i\sum_j G_j\hat{b}_je^{i\beta_j}, \qquad (7)$$

$$\frac{d\hat{b}_j}{dt} = \left(-i\Delta_j - \frac{\gamma}{2}\right)\hat{b}_j - iG_j(\hat{a}_{cw}e^{i\beta_j} + \hat{a}_{ccw}e^{-i\beta_j}), \quad (8)$$

where κ and γ are the dissipation rate of optical fields $\hat{a}_{cw}$ (and $\hat{a}_{ccw}$) and atom ensembles, respectively. This κ consists of the intrinsic dissipation rate of the microtoroid κ_0 and coupling decay rate $\kappa_{1(2)}^{\text{ext}}$. Then, Eq. (8) can be formally integrated as

$$\hat{b}_j(t) = \hat{b}_j(0)e^{(-i\Delta_j - \gamma/2)t} - i\int_0^t G_j[\hat{a}_{cw}(t')e^{i\beta_j} + \hat{a}_{ccw}(t')e^{-i\beta_j}]e^{(-i\Delta_j - \gamma/2)(t-t')}dt'. \qquad (9)$$

The collective bosonic mode $\hat{b}_j$ can be further adiabatically eliminated under the condition that the dissipation γ or the detuning Δ_j are larger than those of optical modes, i.e., $\Delta_j, \gamma \gg \Delta_c, \kappa$. Apparently, the first term of Eq. (9) becomes zero under the high dissipation condition. Since the evolution of optical fields is much slower than atom ensembles, the values of $\hat{a}_{cw}$ and $\hat{a}_{ccw}$ at time t' can be regarded as nearly the same with the values at time t. Therefore, the operators $\hat{a}_{cw}(t')$ and $\hat{a}_{ccw}(t')$ are written as $\hat{a}_{cw}(t)$ and $\hat{a}_{ccw}(t)$, which can be taken out from this integration. Finally, Eq. (9) is derived to be $\hat{b}_j(t) = i\chi_j G_j(\hat{a}_{cw}e^{i\beta_j} + \hat{a}_{ccw}e^{-i\beta_j})$, in which $\chi_j = (-i\Delta_j - \gamma/2)^{-1}$. By taking this result into Eqs. (6) and (7), the evolution of optical fields becomes $d(\hat{a}_{cw}\ \hat{a}_{ccw})^T/dt = M(\hat{a}_{cw}\ \hat{a}_{ccw})^T$, and the matrix M is given by

$$\begin{pmatrix} -i\Delta_c - \frac{\kappa}{2} + \sum_i \chi_j G_j^2 & \sum_j \chi_j G_j^2 e^{-i2\beta_j} \\ \sum_j \chi_j G_j^2 e^{i2\beta_j} & -i\Delta_c - \frac{\kappa}{2} + \sum_j \chi_j G_j^2 \end{pmatrix}. \qquad (10)$$

The diagonal elements of Eq. (10) represent the effective detuning Δ_c' and the damping rate κ' of optical modes, which can be expressed as

$$\Delta_c' = \Delta_c - \sum_j \frac{G_j^2\Delta_j}{\Delta_j^2 + \gamma^2/4}, \qquad (11)$$

$$\kappa' = \kappa + \sum_j \frac{G_j^2\gamma}{\Delta_j^2 + \gamma^2/4}. \qquad (12)$$

Apparently, the changes of Δ_c' and κ' are proportional to the square of coupling strength G_j. That is to say, when Δ_j and γ are kept unchanged, an increase of G_j^2 will lead to the increase of κ' and the reduction of Δ_c'. Next, we focus on the effect of Δ_j on both Δ_c' and κ'. Assuming that we continuously tune the detuning Δ_n of the nth atom ensemble and keep other ensembles unchanged, as shown in Fig. 2, the changes of dissipation rate κ' exhibit symmetric behaviors, while the changes of detuning Δ_c' shows an antisymmetric line shape. Moreover, the existence of more atomic ensembles would increase the dissipation rate of optical fields because more dissipative channels are opened. The changes of Δ_c' and κ' are
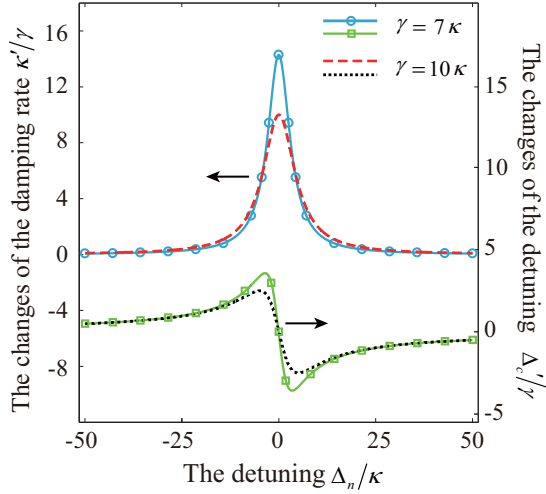
FIG. 2. The changes of effective detunings Δ_c' and dissipation rate κ' when tuning the nth atom ensemble. The blue line (circle symbol) and dashed red line correspond to the changes of κ' with dissipation rate $\gamma/\kappa = 7$ and $\gamma/\kappa = 10$, respectively. Also, the green line (square symbol) and dotted black line demonstrate the changes of Δ_c' with dissipation rate $\gamma/\kappa = 7$ and $\gamma/\kappa = 10$, respectively. The coupling strength between this ensemble and the microtoroid is $G_n/\kappa = 5$.

also related to the dissipation rate γ of atom ensembles. When γ is reduced from 10κ to 7κ, the peak value of the change of κ' becomes higher, and the Fano-like shape of the change of Δ_c' becomes more obvious, which is shown in Fig. 2.

With considering the dissipation of this system, the effective Hamiltonian described by the evolution $\boldsymbol{M}$ is non-Hermitian, which could be expressed as

$$\hat{H}_{\text{eff}} = i \sum_j \chi_j G_j^2 e^{-i2\beta_j} \hat{a}_{cw}^\dagger \hat{a}_{ccw} + i \sum_j \chi_j G_j^2 e^{i2\beta_j} \hat{a}_{cw} \hat{a}_{ccw}^\dagger$$
$$+ \left(\Delta_c' - i \frac{\kappa'}{2} \right) (\hat{a}_{cw}^\dagger \hat{a}_{cw} + \hat{a}_{ccw}^\dagger \hat{a}_{ccw}). \quad (13)$$

Here, the off-diagonal elements $|M_{12}|$ and $|M_{21}|$, which describe the coupling between CW and CCW mode, are not exactly the same. This property leads to the asymmetric backscattering of this system. As shown in Fig. 1(a), when the light is input from port 1 (or port 2), the normalized transmission coupled out from port 3 (or port 4) can be derived as

$$T_{1\to3(2\to4)} = \frac{16|M_{21(12)}|^2 \kappa_1^{\text{ext}} \kappa_2^{\text{ext}}}{|(-2i\Delta_c' - \kappa')^2 - 4M_{12}M_{21}|^2}. \quad (14)$$

Here, κ_1^{ext} and κ_2^{ext} represent the resonator-waveguide coupling strength of this add-drop structure, as shown in Fig. 1(a). When $|M_{12}| \neq |M_{21}|$, the transmissions of $1 \to 3$ and $2 \to 4$ are different. Furthermore, the chirality parameter D is defined to describe the asymmetric backscattering of this system as

$$D = \frac{|M_{21}| - |M_{12}|}{|M_{21}| + |M_{12}|}. \quad (15)$$

It is apparent that when $|M_{21}|$ (or $|M_{12}|$) becomes zero, the chirality becomes 1 (or -1). That is to say, only the CW mode
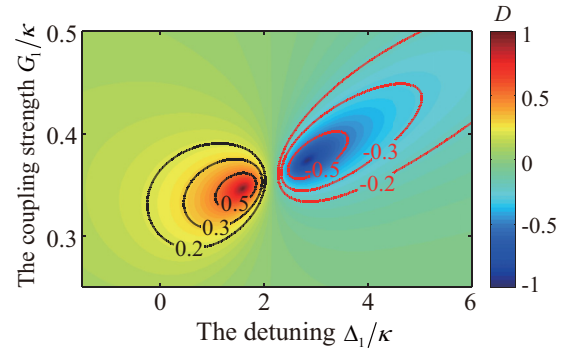
FIG. 3. The changes of chirality D with respect to the detuning Δ_1 and the coupling strength G_1 of the first atom ensemble. Other parameters have values $\kappa_1^{\text{ext}}/\kappa_0 = 2$, $\kappa_2^{\text{ext}}/\kappa_0 = 0.2$, $\gamma/\kappa = 5$, $\Delta_2/\kappa = 15$, $\beta = 0.1\pi$, and $G_2/\kappa = 2$.

(or CCW mode) can couple into the CCW (or CW mode). The requirement for the exact asymmetric backscattering is

$$\sum_j \chi_j G_j^2 e^{+(-)i2\beta_j} = 0. \quad (16)$$

Note that when it is the $+$ (or $-$) symbol, the CW mode (or CCW mode) can only couple into a CCW mode (or CW mode). When the position of the jth atomic ensemble is fixed, χ_j can be faithfully controlled through changing the input frequency of the external field ω_p^j, and the coupling strength G_j can be controlled by modifying the Rabi frequency Ω_j. Therefore, M_{12} or M_{21} can be continuously tuned to make the system into an exact asymmetric backscattering region while keeping the phase β_j unchanged.

In order to show the efficiency of controlling the chirality proposed here, we consider the situation containing two Rydberg-atom ensembles with phase 0 and β, respectively. Under this situation, Eq. (16) evolves into $G_1^2 \chi_1 + G_2^2 \chi_2 \exp\{+(-)2i\beta\} = 0$. Apparently, the real and imaginary part should be zero simultaneously. Here, we define $\cos\alpha_{1(2)} = \gamma/|\gamma + 2i\Delta_{1(2)}|$ and $\sin\alpha_{1(2)} = 2\Delta_{1(2)}/|\gamma + 2i\Delta_{1(2)}|$. When the CW mode can only couple into CCW mode, the coupling strength $G_{1(2)}$ and the detuning $\Delta_{1(2)}$ need to satisfy the following conditions:

$$\Delta_1 = \frac{\gamma}{2} \tan(\alpha_2 + 2\beta), \quad (17)$$

$$G_1^2 |\chi_1| \cos\alpha_1 = G_2^2 |\chi_2| \cos(\alpha_2 + 2\beta). \quad (18)$$

Here, when the $+$ sign is replaced by a $-$ sign, the CCW mode can only couple into a CW mode. The changes of chirality D with respect to the detuning Δ_1 and coupling strength G_1 are shown in Fig. 3. The chirality D exhibits a clear feature of the continuous transition from 1 to -1 by choosing proper Δ_1 and G_1. When the chirality D is 1, $T_{2\to4} = 0$, i.e., the CW mode can couple into the CCW mode. Similarly, when D is -1, $T_{1\to3}$ becomes zero, and only the CCW mode can couple into the CW mode.

To better show the chiral backscattering properties of this system, the normalized transmission spectra are plotted in Fig. 4. Figure 4(a) corresponds to the transmission spectra in the asymmetric backscattering region with $\Delta_1/\gamma = -4.5$.
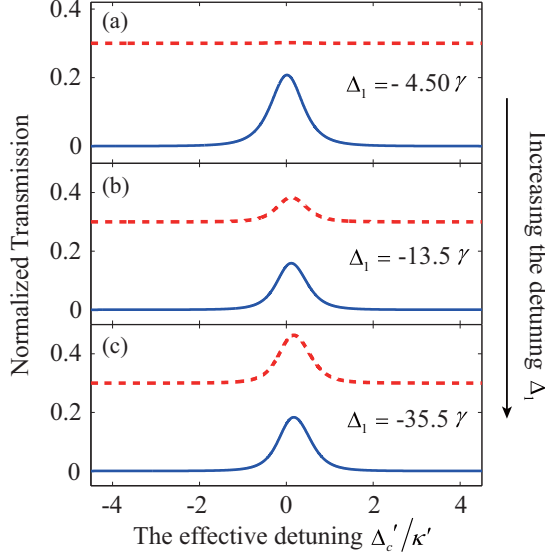
FIG. 4. The evolution of transmission spectra from the asymmetric backscattering region to the nearly symmetric backscattering region. The red dashed line stands for the transmission $T_{2\to4}$, while the blue line represents the transmission $T_{1\to3}$. The value of Δ_1 is -4.5κ in (a), -13.5κ in (b), and -35.5κ in (c). The other parameters are $\Delta_2/\kappa = 15$, $\beta = 0.1\pi$, $G_2/\kappa = 2$, $G_1/\kappa = 1.23$, $\gamma/\kappa = 5$, $\kappa_1^{\text{ext}}/\kappa_0 = 2$, and $\kappa_2^{\text{ext}}/\kappa_0 = 0.2$.

The light can have the transmission from port 2 to port 4. However, no light can couple out with the input from port 1. In this case, only the CCW mode can couple into the CW mode, and the reverse process is not permitted. When Δ_1 is further increased in Figs. 4(b) and 4(c), the transmission spectra of these two opposite directions become more similar, indicating the mutual coupling between the CW and CCW modes.

IV. THE KERR NONLINEARITY AND CONTROLLABLE PHOTON BLOCKADE

In this section, we investigate the statistical properties of photons induced by tunable nonlinear terms inside this system. In 2010, Liew and Savona [57] proposed that two coupled quantum modes with weak nonlinearity can work as a single-photon source. Subsequently, Bamba *et al.* [58] showed that this phenomenon originates from the destructive quantum interference effect between different optical modes. Until now, more properties about photon blockades in coupled-mode systems are well investigated by theory and experiment [59–61]. The system considered here contains two optical modes with Kerr nonlinearity, which can also achieve the unconventional photon blockade according to the results of previous research [57–61]. The difference of this paper lies in that coupling terms between these two optical modes are asymmetric in the above model. In the following, we will show that the equal-time second-order correlation function $g^{(2)}(0)$ can be well controlled through changing this asymmetric interaction of the non-Hermitian Hamiltonian according to the method given in Refs. [58,59].

When considering the nonlinear term, the χ_i becomes $[-i(\Delta_j - J_j^2 \hat{n}/\Delta_p^j) - \gamma/2]^{-1}$ after adiabatically eliminating

atom ensembles. Under the condition that $\gamma \gg \Delta_j$, it becomes $\chi_j = 4i(\Delta_j - J_j^2 \hat{n}/\Delta_p^j)/\gamma^2 - 4/\gamma$ using Taylor series expansion, which indicates that the Hamiltonian contains the Kerr nonlinear terms $\hat{a}_{cw}^\dagger \hat{a}_{cw}^\dagger \hat{a}_{cw} \hat{a}_{cw}$ and $\hat{a}_{ccw}^\dagger \hat{a}_{ccw}^\dagger \hat{a}_{ccw} \hat{a}_{ccw}$ together with the cross Kerr nonlinear term $\hat{a}_{cw}^\dagger \hat{a}_{cw} \hat{a}_{ccw}^\dagger \hat{a}_{ccw}$. This effect can be illustrated through the effective Hamiltonian given by

$$\hat{H}' = \Delta_c'(\hat{a}_{cw}^\dagger \hat{a}_{cw}^\dagger + \hat{a}_{ccw}^\dagger \hat{a}_{ccw}^\dagger) + 2U \hat{a}_{cw}^\dagger \hat{a}_{cw} \hat{a}_{ccw}^\dagger \hat{a}_{ccw}$$
$$+ U(\hat{a}_{cw}^\dagger \hat{a}_{cw}^\dagger \hat{a}_{cw} \hat{a}_{cw} + \hat{a}_{ccw}^\dagger \hat{a}_{ccw}^\dagger \hat{a}_{ccw} \hat{a}_{ccw})$$
$$+ g_{12} \hat{a}_{cw}^\dagger \hat{a}_{ccw} + g_{21} \hat{a}_{cw} \hat{a}_{ccw}^\dagger + \varepsilon'(\hat{a}_{cw}^\dagger + \hat{a}_{cw}). \quad (19)$$

The detuning of CW and CCW modes with respect to the pump laser is rewritten as Δ_c', and the dissipation rate κ' has an expression as $\kappa + 4\sum_j G_j^2/\gamma$. The nonlinear term U is $-4\sum_j G_j^2 J_j^2/(\Delta_p^j \gamma_i^2)$, while the asymmetric coupling terms are $g_{12} = 4i \sum_j G_j^2 (i\Delta_j - \gamma)e^{-2\beta_j i}/\gamma^2$ and $g_{21} = 4i \sum_j G_j^2 (i\Delta_j - \gamma)e^{2\beta_j i}/\gamma^2$.

When we neglect this nonlinear term U, the eigenfrequency of these two supermodes could be solved as

$$\omega_\pm = i\Delta_c' - \frac{\kappa'}{2} \pm i\sqrt{g_{12}g_{21}}. \quad (20)$$

Apparently, the imaginary part of $g_{12}g_{21}$ may not be zero. It would have the expression as $i\Delta_c' - (\kappa' \pm 2\sqrt{|g_{12}g_{21}|})/2$ when $g_{12}g_{21} < 0$. In this case, these two supermodes have the same resonant frequencies, but their dissipation rates are different, which indicates that they cannot be distinguished from the transmission spectra. When $g_{12}g_{21} > 0$, these two supermodes have the same dissipation rate but different resonant frequencies, and $\omega_\pm$ becomes $i(\Delta_c' \pm \sqrt{|g_{12}g_{21}|}) - \kappa'/2$, which can be well separated from the spectrum. Meanwhile, the exceptional point corresponds to the relation $g_{12}g_{21} = 0$, which shows great potential in ultrasensitive detections [50,54].

When the excitation of the optical mode is weak enough, i.e., $\varepsilon' \ll \kappa'$, only the lower excited states can be excited, and the mean number of photons inside the microcavity is relatively small. Assuming that the maximum photon number is less than 2, the state of this system becomes

$$|\psi\rangle = C_{00}|00\rangle + C_{10}|10\rangle + C_{01}|01\rangle + C_{20}|20\rangle$$
$$+ C_{02}|02\rangle + C_{11}|11\rangle. \quad (21)$$

Here, the state $|n_{cw}, n_{ccw}\rangle$ stands for the Fock state in which this system has n_{cw} photons in the CW mode and n_{ccw} photons in the CCW mode. Since the pump is weak enough, the coefficients of this Fock state satisfy the condition $C_{00} \gg C_{10}, C_{01} \gg C_{20}, C_{11}, C_{02}$. The evolution of this system can be solved in this subspace, which follows the Schrodinger equation

$$i\hbar \frac{\partial |\psi\rangle}{\partial t} = \hat{H}|\psi\rangle. \quad (22)$$
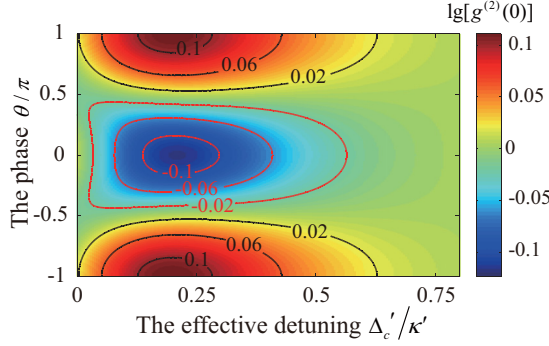
FIG. 5. The changes of the equal-time second-order correlation function $g^{(2)}(0)$ vs the phase θ and detuning Δ'_c. The values of other parameters are $\varepsilon'/\kappa' = 0.01$, $U/\kappa' = 0.005$, and $g/\kappa' = 3$.

Under the steady-state condition, these coefficients can be derived as

$$C_{10} = -\frac{\varepsilon' C_{00}}{\Xi_0^{-1} - g_{12}g_{21}\Xi_0}, \tag{23}$$

$$C_{20} = -\frac{2 + g_{12}g_{21}(\Xi_0 - \Xi_1)\Xi_1}{\sqrt{2}(\Xi_1^{-1} - g_{12}g_{21}\Xi_1)}\varepsilon' C_{10}, \tag{24}$$

in which $\Xi_0 = (\Delta'_c - i\kappa'/2)^{-1}$ and $\Xi_1 = (\Delta'_c - i\kappa'/2 + U)^{-1}$. With a weak pump, the term $C_{00} \to 1$ and the second-order correlation function $g^{(2)}(0)$ can be obtained as

$$g^{(2)}(0) \simeq \frac{2|C_{20}|^2}{|C_{10}|^4}. \tag{25}$$

It is obvious as seen from Eqs. (23)–(25) that the photon statistics is determined by the product of g_{12} and g_{21} rather than their individual values. Here, $g_{12}g_{21}$ is rewritten as $g^2 e^{i\theta}$ for simplicity, in which g is the effective coupling strength and θ is the total phase factor.

In Fig. 5, we plot the correlation function $g^{(2)}(0)$ as a function of θ and the detuning Δ'_c while g is kept unchanged. This figure is calculated from the master equation in the Lindblad form $\dot{\rho}(t) = i[\rho(t), \hat{H}'] - \kappa'[\mathcal{L}(\hat{a}_{cw}) + \mathcal{L}(\hat{a}_{ccw})]\rho(t)$, and $\mathcal{L}(o)\rho = \frac{1}{2}(o^\dagger o\rho + \rho o^\dagger o) - o\rho o^\dagger$. As shown in Fig. 5(a), when the phase θ is zero, $g^{(2)}(0) < 1$, which shows the strong photon blockade effect. When θ is increased from 0 to π (or decreases to $-\pi$), $g^{(2)}(0)$ will increase (or decrease) simultaneously. Actually, the number of photons in $|10\rangle$ state originates from the interference from the $|01\rangle$ state and $|00\rangle$ state. Meanwhile, the photon in the $|20\rangle$ state is determined by the interference from the $|11\rangle$ and $|10\rangle$ states. Therefore the phase factor θ and the coupling strength g play important roles during this process.

When $g^{(2)}(0) = 0$, this chiral microresonator can be used as the perfect single-photon source. By setting C_{20} to be zero, the condition is given by

$$4\Delta'_c U^2 + \left(8\Delta'^2_c - 2\kappa'^2 + 2g^2\cos\theta\right)U + 4\Delta'^3_c = 3\Delta'_c\kappa'^2, \tag{26}$$

$$\left(12\Delta'^2_c + 16\Delta'_c U + 4U^2 - \kappa'^2\right)\kappa' - 4g^2 U\sin\theta = 0. \tag{27}$$
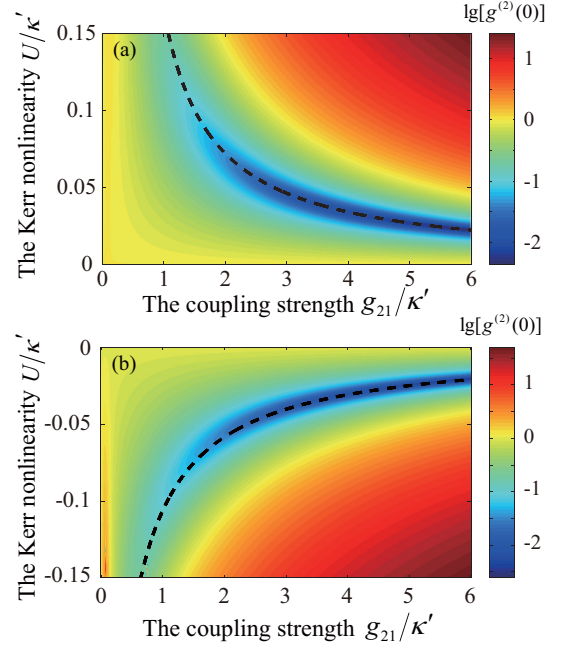
FIG. 6. The changes of the equal-time second-order correlation function $g^{(2)}(0)$ vs the coupling strength g_{21} and U with phase $\theta = 0$ in (a) and $\theta = \pi$ in (b). The dashed lines are the optical U_{opt} calculated from Eq. (29). The detuning Δ'_c is chosen as $\kappa'/(2\sqrt{3})$. The values of other parameters are $\varepsilon'/\kappa' = 0.01$ and $g_{12}/\kappa' = 3$.

These conditions are coincident with the results in Ref. [58]. As the Kerr nonlinearity U is weak enough, the optimal solution for Eqs. (26) and (27) becomes

$$\Delta'^{\text{opt}}_c \simeq \pm\frac{\kappa'}{2\sqrt{3}}, \tag{28}$$

$$U^{\text{opt}} \simeq \pm\frac{2\kappa'^3}{\sqrt{3}(3g^2\cos\theta - 2\kappa'^2)}. \tag{29}$$

The changes of $g^{(2)}(0)$ with respect to the coupling strength g and the Kerr nonlinearity U are shown in Fig. 6. It can be observed that with the increase of g_{21} (i.e., g), the minimum value of $g^{(2)}(0)$ becomes smaller, and the optimal U_{opt} decreases simultaneously. The black dashed lines are calculated from Eq. (29), which denotes the optimal parameter, and it can fit well with the numerical calculation. As analyzed above, the population of each is determined by interferences from nearby states. The increase of g would enhance this interference, and also the photon blockade effect.

V. CONCLUSION

To conclude, we have achieved a chiral whispering gallery mode microresonator assisted by Rydberg-atom ensembles. The chirality of the system can be well controlled by changing the input frequency and strength of the external control field acting on atom ensembles while the position of the ensemble is kept unchanged. The microresonator exhibits asymmetric backscattering due to the chiral light-matter interaction, which has significant applications in optical diodes or optical routers. Meanwhile, the controllable photon blockade can also be

achieved by tuning the coupling phase and strength in this chiral interaction.

APPENDIX: THE ANALYTICAL SOLUTION OF THE SCHRÖDINGER EQUATION IN SEC. IV

First, we consider the one-photon excitation states, i.e., $|10\rangle$ and $|01\rangle$ states. The evolution of these two states can be described as

$$i\frac{\partial C_{10}}{\partial t} = \left(\Delta_c' - i\frac{\kappa'}{2}\right)C_{10} + g_{12}C_{01} + \varepsilon'C_{00}, \quad \text{(A1)}$$

$$i\frac{\partial C_{01}}{\partial t} = \left(\Delta_c' - i\frac{\kappa'}{2}\right)C_{01} + g_{21}C_{10}. \quad \text{(A2)}$$

Under the steady-state condition, this amplitude can be obtained as $C_{01} = -\Xi_0 g_{21} C_{10}$, and

$$C_{10} = -\frac{\varepsilon'C_{00}}{\Xi_0^{-1} - g_{12}g_{21}\Xi_0}. \quad \text{(A3)}$$

Next, we consider the evolution of two-photon excitation states, i.e., the $|20\rangle$, $|11\rangle$, and $|02\rangle$ states. From the Eq. (22), the evolution of these states can be given by

$$i\frac{\partial C_{20}}{\partial t} = (2\Delta_c' - i\kappa' + 2U)C_{20} + \sqrt{2}\varepsilon'C_{10} + \sqrt{2}g_{12}C_{11}, \quad \text{(A4)}$$

$$i\frac{\partial C_{02}}{\partial t} = (2\Delta_c' - i\kappa' + 2U)C_{02} + \sqrt{2}g_{21}C_{11}, \quad \text{(A5)}$$

$$i\frac{\partial C_{11}}{\partial t} = (2\Delta_c' - i\kappa' + 2U)C_{11} + \varepsilon'C_{01} + \sqrt{2}g_{21}C_{20}$$
$$+ \sqrt{2}g_{12}C_{02}. \quad \text{(A6)}$$

The $|02\rangle$ state can be adiabatically eliminated in the steady-state situation. According to Eq. (27), we can get that $2C_{02} = -\sqrt{2}g_{21}C_{11}\Xi_1$. Taking this formula into Eqs. (A4) and (A6), their evolutions become

$$i\frac{\partial C_{20}}{\partial t} = 2\Xi_1^{-1}C_{20} + \sqrt{2}g_{12}C_{11} + \sqrt{2}\varepsilon'C_{10}, \quad \text{(A7)}$$

$$i\frac{\partial C_{11}}{\partial t} = \left(2\Xi_1^{-1} - g_{12}g_{21}\Xi_1\right)C_{11} + \sqrt{2}g_{21}C_{20}$$
$$- g_{21}\Xi_0\varepsilon'C_{10}. \quad \text{(A8)}$$

Furthermore, we can get the $|11\rangle$ state as

$$C_{11} = \frac{g_{21}(\Xi_1 + \Xi_0)}{2\left(\Xi_1^{-1} - g_{12}g_{21}\Xi_1\right)}\varepsilon'C_{10}. \quad \text{(A9)}$$

From the above analyses, the transition between different energy levels can be simplified by eliminating the $|10\rangle \leftrightarrow |01\rangle$ and the $|11\rangle \leftrightarrow |02\rangle$ transitions. The population of the $|20\rangle$ state results from the interference between the $|11\rangle$ state and $|10\rangle$ state, i.e., $C_{20} \propto g_{12}C_{11} + \varepsilon'C_{10}$. The C_{20} could be expressed as

$$C_{20} = -\frac{2 + g_{12}g_{21}(\Xi_0 - \Xi_1)\Xi_1}{\sqrt{2}\left(\Xi_1^{-1} - g_{12}g_{21}\Xi_1\right)}\varepsilon'C_{10}. \quad \text{(A10)}$$

When C_{20} approaches zero, the optimal condition derived from Eqs. (A4)–(A6) becomes

$$\begin{vmatrix} 0 & g_{12} & \varepsilon' \\ 2\,\Xi_1^{-1} & \sqrt{2}g_{21} & 0 \\ \sqrt{2}g_{12} & 2\,\Xi_1^{-1} & \varepsilon'g_{21}\Xi_0^{-1} \end{vmatrix} = 0 \quad \text{(A11)}$$

or

$$\Delta_c'[4(\Delta_c' + U)^2 - \kappa'^2] - 2\kappa'^2(\Delta_c' + U) + 2g_{12}g_{21}U$$
$$- 4i\Delta_c'\kappa'(\Delta_c' + U) - 2i\kappa'(\Delta_c' + U)^2 - i\frac{\kappa'^3}{2} = 0. \quad \text{(A12)}$$

Therefore, when both the real and imaginary parts of Eq. (A12) are set to be zero, Eqs. (26) and (27), demonstrated in Sec. IV, can be obtained.

[1] D. R. Yennie, Rev. Mod. Phys. **59**, 781 (1987).

[2] M. Endres, T. Fukuhara, D. Pekker, M. Cheneau, P. Schaub, C. Gross, E. Demler, S. Kuhr, and I. Bloch, Nature (London) **487**, 454 (2012).

[3] T. Zibold, E. Nicklas, C. Gross, and M. K. Oberthaler, Phys. Rev. Lett. **105**, 204101 (2010).

[4] M. König, S. Wiedmann, C. Brüne, A. Roth, H. Buhmann, L. W. Molenkamp, X.-L. Qi, and S.-C. Zhang, Science **318**, 766 (2007).

[5] I. Serban, B. Béri, A. R. Akhmerov, and C. W. J. Beenakker, Phys. Rev. Lett. **104**, 147001 (2010).

[6] P. Lodahl, S. Mahmoodian, S. Stobbe, A. Rauschenbeutel, P. Schneeweiss, J. Volz, H. Pichler, and P. Zoller, Nature (London) **541**, 473 (2017).

[7] K. Y. Bliokh and F. Nori, Phys. Rep. **592**, 1 (2015).

[8] K. Y. Bliokh, F. J. Rodríguez-Fortuño, F. Nori, and A. V. Zayats, Nat. Photonics **9**, 796 (2015).

[9] A. Aiello, P. Banzer, M. Neugebauer, and G. Leuchs, Nat. Photonics **9**, 789 (2015).

[10] C. Junge, D. OShea, J. Volz, and A. Rauschenbeutel, Phys. Rev. Lett. **110**, 213604 (2013).

[11] M. Lax, W. H. Louisell, and W. B. McKnight, Phys. Rev. A **11**, 1365 (1975).

[12] K. Y. Bliokh and F. Nori, Phys. Rev. A **85**, 061801 (2012).

[13] R. J. Coles, N. Prtljaga, B. Royall, I. J. Luxmoore, A. M. Fox, and M. S. Skolnick, Opt. Express **22**, 2376 (2014).

[14] J. Petersen, J. Volz, and A. Rauschenbeutel, Science **346**, 67 (2014).

[15] I. Shomroni, S. Rosenblum, Y. Lovsky, O. Bechler, G. Guendelman, and B. Dayan, Science **345**, 903 (2014).

[16] C. Sayrin, C. Junge, R. Mitsch, B. Albrecht, D. OShea, P. Schneeweiss, J. Volz, and A. Rauschenbeutel, Phys. Rev. X **5**, 041036 (2015).

[17] D. K. Armani, T. J. Kippenberg, S. M. Spillane, and K. J. Vahala, Nature (London) **421**, 925 (2003).

[18] B. Dayan, A. S. Parkins, T. Aoki, E. P. Ostby, K. J. Vahala, and H. J. Kimble, Science **319**, 1062 (2008).

[19] V. B. Braginsky, M. L. Gorodetsky, and V. S. Ilchenko, Phys. Lett. A **137**, 393 (1989).

[20] T. Carmon, L. Yang, and K. J. Vahala, Opt. Express **12**, 4742 (2004).

[21] K. Totsuka and M. Tomita, Opt. Lett. **32**, 3197 (2007).

[22] X.-F. Liu, F. Lei, M. Gao, X. Yang, G.-Q. Qin, and G.-L. Long, Opt. Lett. **41**, 3603 (2016).

[23] K. J. Vahala, Nature (London) **424**, 839 (2003).

[24] L. Yang, D. K. Armani, and K. J. Vahala, Appl. Phys. Lett. **83**, 825 (2003).

[25] B. Min, T. J. Kippenberg, L. Yang, K. J. Vahala, J. Kalkman, and A. Polman, Phys. Rev. A **70**, 033803 (2004).

[26] V. Sandoghdar, F. Treussart, J. Hare, V. Lefèvre-Seguin, J.-M. Raimond, and S. Haroche, Phys. Rev. A **54**, R1777(R) (1996).

[27] B. Peng, Ş. K. Özemdir, F. Lei, F. Monifi, M. Gianfreda, G. L. Long, S. Fan, F. Nori, C. M. Bender, and L. Yang, Nat. Phys. **10**, 394 (2014).

[28] L. Chang, X. Jiang, S. Hua, C. Yang, J. Wen, L. Jiang, G. Li, G. Wang, and M. Xiao, Nat. Photonics **8**, 524 (2014).

[29] L. Feng, Z. J. Wong, R.-M. Ma, Y. Wang, and X. Zhang, Science **346**, 972 (2014).

[30] H. Hodaei, M.-A. Miri, M. Heinrich, D. N. Christodoulides, and M. Khajavikhan, Science **346**, 975 (2014).

[31] P. Peng, W. Cao, C. Shen, W. Qu, J. Wen, L. Jiang, and Y. Xiao, Nat. Phys. **12**, 1139 (2016).

[32] S. M. Spillane, T. J. Kippenberg, K. J. Vahala, K. W. Goh, E. Wilcut, and H. J. Kimble, Phys. Rev. A **71**, 013817 (2005).

[33] Y.-S. Park and H. Wang, Nat. Phys. **5**, 489 (2009).

[34] S. Weis, R. Rivière, S. Deléglise, E. Gavartin, O. Arcizet, A. Schliesser, and T. J. Kippenberg, Science **330**, 1520 (2010).

[35] T. Carmon, H. Rokhsari, L. Yang, T. J. Kippenberg, and K. J. Vahala, Phys. Rev. Lett. **94**, 223902 (2005).

[36] F. Monifi, J. Zhang, Ş. K. Özdemir, B. Peng, Y. xi Liu, F. Bo, F. Nori, and L. Yang, Nat. Photonics **10**, 399 (2016).

[37] Z. Shen, Y.-L. Zhang, Y. Chen, C.-L. Zou, Y.-F. Xiao, X.-B. Zou, F.-W. Sun, G.-C. Guo, and C.-H. Dong, Nat. Photonics **10**, 657 (2016).

[38] T. J. Kippenberg, R. Holzwarth, and S. A. Diddams, Science **332**, 555 (2011).

[39] F. Bo, J. Wang, J. Cui, Ş. K. Özdemir, Y. Kong, G. Zhang, J. Xu, and L. Yang, Adv. Mater. **27**, 8075 (2015).

[40] Q.-T. Cao, H. Wang, C.-H. Dong, H. Jing, R.-S. Liu, X. Chen, L. Ge, Q. Gong, and Y.-F. Xiao, Phys. Rev. Lett. **118**, 033901 (2017).

[41] V. Huet, A. Rasoloniaina, P. Guillemé, P. Rochard, P. Féron, M. Mortier, A. Levenson, K. Bencheikh, A. Yacomotti, and Y. Dumeige, Phys. Rev. Lett. **116**, 133902 (2016).

[42] J. Zhu, S. K. Ozdemir, Y.-F. Xiao, L. Li, L. He, D.-R. Chen, and L. Yang, Nat. Photonics **4**, 46 (2010).

[43] Y. Zhi, X.-C. Yu, Q. Gong, L. Yang, and Y.-F. Xiao, Adv. Mater. **29**, 1604920 (2017).

[44] T. Reynolds, N. Riesen, A. Meldrum, X. Fan, J. M. M. Hall, T. M. Monro, and A. François, Laser Photonics Rev. **11**, 1600265 (2017).

[45] M. Scheucher, A. Hilico, E. Will, J. Volz, and A. Rauschenbeutel, Science **354**, 1577 (2016).

[46] K. Xia, G. Lu, G. Lin, Y. Cheng, Y. Niu, S. Gong, and J. Twamley, Phys. Rev. A **90**, 043802 (2014).

[47] L. Feng, R. El-Ganainy, and L. Ge, Nat. Photonics **11**, 752 (2017).

[48] H. Schomerus and J. Wiersig, Phys. Rev. A **90**, 053819 (2014).

[49] J. Wiersig, Phys. Rev. A **84**, 063828 (2011).

[50] J. Wiersig, Phys. Rev. A **93**, 033809 (2016).

[51] J. Wiersig, Phys. Rev. Lett. **112**, 203901 (2014).

[52] B. Peng, Ş. K. Özdemir, M. Liertzer, W. Chen, J. Kramer, H. Yilmaz, J. Wiersig, S. Rotter, and L. Yang, Proc. Natl. Acad. Sci. USA **113**, 6845 (2016).

[53] M. Kim, K. Kwon, J. Shim, Y. Jung, and K. Yu, Opt. Lett. **39**, 2423 (2014).

[54] W. Chen, Ş. K. Özdemir, G. Zhao, J. Wiersig, and L. Yang, Nature (London) **548**, 192 (2017).

[55] J. Zhu, Ş. K. Özdemir, L. He, and L. Yang, Opt. Express **18**, 23535 (2010).

[56] X. Yi, Y.-F. Xiao, Y.-C. Liu, B.-B. Li, Y.-L. Chen, Y. Li, and Q. Gong, Phys. Rev. A **83**, 023803 (2011).

[57] T. C. H. Liew and V. Savona, Phys. Rev. Lett. **104**, 183601 (2010).

[58] M. Bamba, A. Imamoğlu, I. Carusotto, and C. Ciuti, Phys. Rev. A **83**, 021802(R) (2011).

[59] X.-W. Xu and Y. Li, Phys. Rev. A **90**, 033809 (2014).

[60] J. Tang, W. Geng, and X. Xu, Sci. Rep. **5**, 9252 (2015).

[61] H. Flayac, D. Gerace, and V. Savona, Sci. Rep. **5**, 11223 (2015).